ELSEVIER

Cryogenics 42 (2002) 49–57

Cryogenics

www.elsevier.com/locate/cryogenics

Design of thermoacoustic refrigerators

M.E.H. Tijani, J.C.H. Zeegers, A.T.A.M. de Waele *

Department of Applied Physics, Eindhoven University of Technology, P.O. Box 513, 5600 MB Eindhoven, Netherlands

Received 12 November 2001; accepted 5 December 2001

Abstract

In this paper the design of thermoacoustic refrigerators, using the linear thermoacoustic theory, is described. Due to the large number of parameters, a choice of some parameters along with dimensionless independent variables will be introduced. The design strategy described in this paper is a guide for the design and development of thermoacoustic coolers. The optimization of the different parts of the refrigerator will be discussed, and criteria will be given to obtain an optimal system.

Keywords: Thermoacoustic; Refrigeration

1. Introduction

The theory of thermoacoustics is well established, but quantitative engineering approach to design thermoacoustic refrigerators is still lacking in the literature. Thermoacoustic refrigerators are systems which use sound to generate cooling power. They consist mainly of a loudspeaker attached to an acoustic resonator (tube) filled with a gas. In the resonator, a stack consisting of a number of parallel plates and two heat exchangers, are installed, as shown in Fig. 1. The loudspeaker sustains an acoustic standing wave in the gas at the fundamental resonance frequency of the resonator. The acoustic standing wave displaces the gas in the channels of the stack while compressing and expanding. The thermal interaction between the oscillating gas and the surface of the stack generates an acoustic heat pumping. The heat exchangers exchange heat with the surroundings, at the cold and hot sides of the stack. A detailed explanation of the way thermoacoustic coolers work is given by Swift [1] and Wheatly et al. [2]. In this paper the design and development procedure of a thermoacoustic refrigerator is reported. The thermoacoustic refrigerator, constructed on basis of the design procedure given in this paper, has operated properly and it has reached a low temperature of −65 °C. The measurement results can be found elsewhere [3,4].

2. Design strategy

We start by considering the design and optimization of the stack which forms the heart of the cooler. The coefficient of performance of the stack, defined as the ratio of the heat pumped by the stack to the acoustic power used by the stack, is to be maximized. The exact theoretical expressions of the acoustic power and cooling power in the stack are complicated, so one can try to use the simplified expressions deduced from the short stack, and boundary-layer approximations [1,3]. These expressions still look complicated and they contain a large number of parameters of the working gas, material and geometrical parameters of the stack. It is difficult to deal in engineering with so many parameters. However, one can reduce the number of parameters by choosing a group of dimensionless independent variables. Olson and Swift [5] wrote a paper about similitude and dimensionless parameters for thermoacoustic devices. Some dimensionless parameters can be deduced directly. Others can be defined from the boundary-layer and short-stack assumptions [1,3]. The parameters, of importance in thermoacoustics, which are contained in the work flow and heat flow expressions are given in Table 1 [3].

The goal of the design of the thermoacoustic refrigerator is to meet the requirements of a given cooling power $\dot{Q}_c$ and a given low temperature T_C. This

* Corresponding author. Tel.: +31-40-247-4215; fax: +31-40-243-8272.

E-mail address: a.t.a.m.d.waele@tue.nl (A.T.A.M. de Waele).

0011-2275/02/$ - see front matter
PII: S0011-2275(01)00179-5

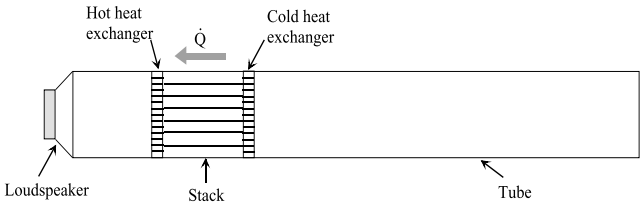

Fig. 1. A simple illustration of a thermoacoustic refrigerator. An acoustically resonant tube containing a gas, a stack of parallel plates and two heat exchangers. A loudspeaker is attached to one end of the tube and the other end is closed. Heat $\dot{Q}$ is pumped up the stack so that the cold heat exchanger becomes colder and the hot heat exchanger hotter.

Table 1
Operation-, working gas-, and stack parameters

Operation parameters	Working gas parameters
Operating frequency: f	Dynamic viscosity: μ
Average pressure: p_m	Thermal conductivity: K
Dynamic pressure amplitude: p_0	Sound velocity: a
Mean temperature: T_m	Ratio of isobaric to isochoric specific heats: γ
Stack	
Material	Geometry
	Length: L_s
Thermal conductivity: K_s	Stack center position: x_s
Density: ρ_s	Plate thickness: $2l$
Specific heat: c_s	Plate spacing: $2y_0$
	Cross-section: A

requirement can be added to the operation parameters shown in Table 1.

The boundary-layer and short-stack approximations assume the following [1,3]:

- The reduced acoustic wavelength is larger than the stack length: $\lambda/2\pi \gg L_s$, so that the pressure and velocity can be considered as constant over the stack and that the acoustic field is not significantly disturbed by the presence of the stack.
- The thermal and viscous penetration depths are smaller than the spacing in the stack: $\delta_k, \delta_v \ll y_0$. This assumption leads to the simplification of Rott's functions, where the complex hyperbolic tangents can be set equal to one [1,3].
- The temperature difference is smaller than the average temperature: $\Delta T_m \ll T_m$, so that the thermophysical properties of the gas can be considered as constant within the stack.

The length and position of the stack can be normalized by $\lambda/2\pi$. The thermal and viscous penetration depths can be normalized by the half spacing in the stack y_0. The cold temperature or the temperature difference can be normalized by T_m. Since δ_k and δ_v (see below) are related by the Prandtl number σ, this will further simplify the number of parameters. Olson and Swift [5] proposed to normalize the acoustic power $\dot{W}$ and the cooling power $\dot{Q}_c$ by the product of the mean pressure p_m, the sound velocity a, and the cross-sectional area of the stack A: $p_m aA$. The amplitude of the dynamic pressure can be normalized by the mean pressure. The ratio p_0/p_m is called the drive ratio D. In practice the stack material can be chosen so that the thermal conductive term in the heat flow expression can be neglected [1]. In this case the parameters of the stack material do not have to be considered in the performance calculations. The porosity of the stack, sometimes called blockage ratio and defined as

$$B = \frac{y_0}{y_0 + l} \tag{1}$$

is also used as a dimensionless parameter for the geometry of the stack. The thermal and viscous penetration depths are given by

$$\delta_k = \sqrt{\frac{2K}{\rho c_p \omega}} \tag{2}$$

and

$$\delta_v = \sqrt{\frac{2\mu}{\rho\omega}}, \tag{3}$$

where K is the thermal conductivity, μ is the viscosity, ρ is the density, c_p is the isobaric specific heat of the gas, and ω is the angular frequency of the sound wave.

The resultant normalized parameters are given an extra index n and are shown in Table 2. The number of parameters can once more be reduced, by making a choice of some operation parameters, and the working gas.

3. Design choices

For this investigation we choose to design a refrigerator for a temperature difference of $\Delta T_m = 75$ K and a cooling power of 4 W. In the following, we will discuss

Table 2
Normalized operation-, working gas-, and stack parameters

Operation parameters
Drive ratio: $D = p_0/p_m$
Normalized cooling power: $Q_{cn} = \dot{Q}_c/p_m aA$
Normalized acoustic power: $W_n = \dot{W}/p_m aA$
Normalized temperature difference: $\Delta T_{mn} = \Delta T_m/T_m$
Gas parameters
Prandtl number: σ
Normalized thermal penetration depth: $\delta_{kn} = \delta_k/y_0$
Stack geometry parameters
Normalized stack length: $L_{sn} = kL_s$
Normalized stack position: $x_n = kx$
Blockage ratio or porosity: $B = y_0/(y_0 + l)$

the selection of some operation parameters, the gas and stack material.

3.1. Average pressure

Since the power density in a thermoacoustic device is proportional to the average pressure p_m [1], it is favorable to choose p_m as large as possible. This is determined by the mechanical strength of the resonator. On the other hand, δ_k is inversely proportional to square root of p_m, so a high pressure results in a small δ_k and a small stack plate spacing. This makes the construction difficult. Taking into account these effects and also making the preliminary choice for helium as the working gas (see below), the maximal pressure is 12 bar. We choose to use 10 bar. To minimize the heat conduction from the hot side of the stack to the cold side, we used a holder made of a material with low thermal conductivity (e.g. POM-Ertacetal).

3.2. Frequency

As the power density in the thermoacoustic devices is a linear function of the acoustic resonance frequency [1] an obvious choice is thus a high resonance frequency. On the other hand δ_k is inversely proportional to the square root of the frequency which again implies a stack with very small plate spacing. Making a compromise between these two effects and the fact that the driver resonance has to be matched to the resonator resonance for high efficiency of the driver, we choose to use a frequency of 400 Hz.

3.3. Dynamic pressure

The dynamic pressure amplitude p_0 is limited by two factors namely, the maximum force of the driver and non-linearities. The acoustic Mach number, defined as

$$M = \frac{p_0}{\rho_m a^2}, \tag{4}$$

has to be limited to $M \approx 0.1$ for gases in order to avoid nonlinear effects [1]. From many experimental studies on the structure of turbulent oscillatory flows, it has unanimously been observed that transition to turbulence in the boundary layer took place at a Reynolds number (R_y) based on Stokes boundary-layer thickness, of about 500–550, independent of the particular flow geometry (pipe, channel, oscillating plate) [6–9]. Since we intend to design a refrigerator with moderate cooling power we will use driving ratios $D < 3\%$, so that $M < 0.1$ and $R_y < 500$.

3.4. Working gas

Helium is used as working gas. The reason for this choice is that helium has the highest sound velocity and thermal conductivity of all inert gases. Furthermore, helium is cheap in comparison with the other noble gases. A high thermal conductivity is wise since δ_k is proportional to the square root of the thermal conductivity coefficient K. The effect of using other gases is discussed elsewhere [10].

3.5. Stack material

The heat conduction through the stack material and gas in the stack region has a negative effect on the performance of the refrigerator [1,3]. The stack material must have a low thermal conductivity K_s and a heat capacity c_s larger than the heat capacity of the working gas, in order that the temperature of the stack plates is steady. The material Mylar is chosen, as it has a low heat conductivity (0.16 W/m K) and is produced in many thicknesses between 10 and 500 μm.

3.6. Stack geometry

There are many geometries which the stack can have: parallel plates, circular pores, pin arrays, triangular pores, etc. The geometry of the stack is expressed in Rott's function f_k. This function is given for some channel geometries in the literature [11]. It is shown that the cooling power is proportional to $\mathrm{Im}(-f_k)$ [11,12]. Fig. 2 shows the real and imaginary parts of f_k for some geometries as functions of the ratio the hydraulic radius r_h and the thermal penetration depth. The hydraulic radius is defined as the ratio of the cross-sectional area and the perimeter of the channel. Pin arrays stacks are the best, but they are too difficult to manufacture.

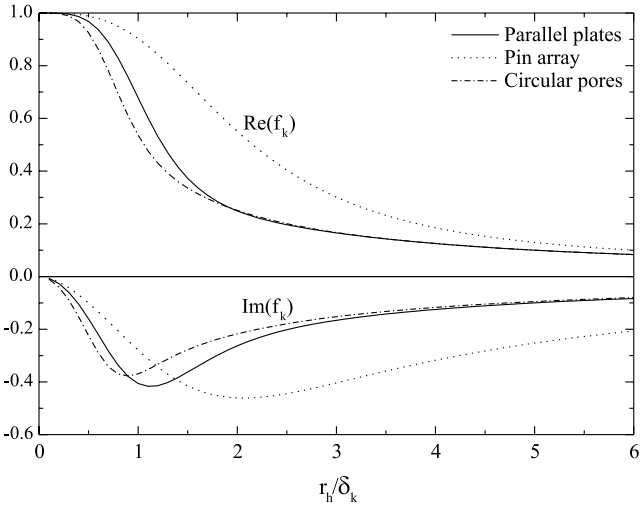

Fig. 2. Imaginary and real parts of the Rott function f_k as function of the ratio of the hydraulic radius and the thermal penetration depth. Three geometries are considered. The pin arrays and parallel-plates stacks are the best. For pin arrays an internal radius $r_i = 3\delta_k$ is used in the calculations.

Hence, we choose to use a stack made of parallel-plates. We note that for parallel-plate stack $r_h = y_0$.

The selection of a frequency of 400 Hz, an average pressure of 10 bar, and helium as working gas, determines the thermal and viscous penetration depths. Using Eqs. (2) and (3) we have for our system $\delta_k = 0.1$ mm and $\delta_v = 0.08$ mm. As can be seen from Fig. 2 for a parallel-plates stack $\mathrm{Im}(-f_k)$ has a maximum for $r_h/\delta_k = y_0/\delta_k = 1.1$. Since the spacing in the stack is $2y_0$, this means that the optimal spacing is 0.22 mm. Using an analogous analysis Arnott et al. [12] obtained an optimal spacing of about 0.26 mm. In order not to alter the acoustic field, it was stated to use a spacing of $2\delta_k$ to $4\delta_k$ [2]. We choose to use a spacing of about 0.3 mm. The experimental study of the effect of the pore dimensions in the stack on the performance of the refrigerator is reported elsewhere [13].

The remaining stack geometrical parameters are the center stack position x_s, the length of the stack L_s, and the cross-sectional area A. These parameters are determined from the performance optimization of the stack.

4. Design of the stack

We remain with three main stack design parameters: the center position x_n, the length L_{sn}, and the cross-sectional area A. This area is equal to the resonator cross-section at the stack location. By using data for the gas parameters we first optimize the stack geometry parameters by optimizing the performance expressed in terms of the coefficient of performance (COP) which is the ratio of the heat pumped by the stack to the acoustic power used to accomplish the heat transfer [3]. This leads to the determination of x_n and L_{sn}. Then the required cooling power will be used to determine the cross-sectional area A. Once these parameters are determined we can design the resonator.

The dissipated acoustic power at the cold side of the resonator forms an extra heat load to the cold heat exchanger. This load, and the required cooling power, will form the total heat load that the cold heat exchanger has to transfer to the stack. The first law of thermodynamics states that the total heat load at the hot heat exchanger is the sum of the heat pumped by the stack and the acoustic power used by the stack to realize the heat transfer process [3]. The hot heat exchanger has to remove this heat from the hot side of the stack. The driver has to provide acoustic power for driving the thermoacoustic heat transport process and compensating for all viscous and thermal dissipation processes in the stack, heat exchangers, and at the resonator wall [3]. The design strategy is summarized in Fig. 3. A detailed outline of the derivation of the expressions given in this paper can be found elsewhere [3].

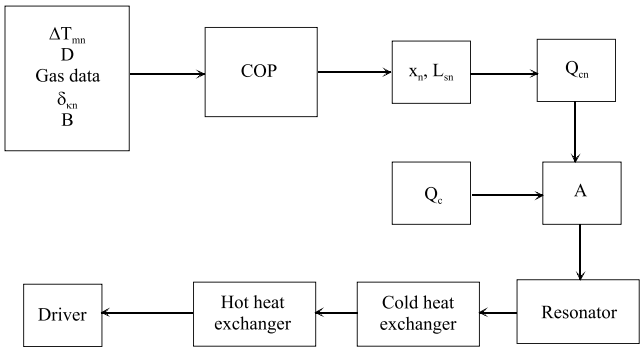

Fig. 3. Illustration of the design procedure of the refrigerator. The stack parameters x_{sn} and L_{sn} are first determined by optimizing the COP. Then A is determined via the required cooling power. After that the resonator is designed, followed by the design of the heat exchangers. The driver has to provide the total needed acoustic power.

Using the dimensionless parameters, the ratio of the temperature gradient along the stack and the critical temperature gradient given by [1]

$$\Gamma = \frac{\nabla T_{\mathrm{m}}}{\nabla T_{\mathrm{c}}}$$

can be rewritten as

$$\Gamma = \frac{\Delta T_{\mathrm{m}n}}{(\gamma - 1)BL_{sn}} \tan(x_n). \tag{5}$$

The stack perimeter, Π, can be expressed as function of the cross-sectional area as

$$\Pi = \frac{A}{y_0 + l}. \tag{6}$$

The expressions of the heat flow and acoustic power can be rewritten in a dimensionless form by using the dimensionless parameters, the gas data of Table 3, and substitution of Eqs. (5) and (6). The result is

$$Q_{cn} = -\frac{\delta_{kn} D^2 \sin 2x_n}{8\gamma(1+\sigma)\Lambda} \times \left(\frac{\Delta T_{\mathrm{m}n} \tan(x_n)}{(\gamma - 1)BL_{sn}} \frac{1 + \sqrt{\sigma} + \sigma}{1 + \sqrt{\sigma}} - \left(1 + \sqrt{\sigma} - \sqrt{\sigma}\delta_{kn}\right) \right) \tag{7}$$

Table 3
Data used in the performance calculations

Operation parameters	Gas parameters
$p_{\mathrm{m}} = 10$ bar	$a = 935$ m/s
$T_{\mathrm{m}} = 250$ K	$\sigma = 0.68$
$\Delta T_{\mathrm{m}n} = 0.3$	$\gamma = 1.67$
$D = 0.02$	$B = 0.75$
$f = 400$ Hz, $k = 2.68$ m^{-1}	$\delta_{kn} = 0.66$

and

$$W_n = \frac{\delta_{kn} L_{sn} D^2}{4\gamma}(\gamma - 1) B \cos^2 x_n \times \left(\frac{\Delta T_{mn} \tan(x_n)}{B L_{sn}(\gamma - 1)(1 + \sqrt{\sigma})\Lambda} - 1 \right) - \frac{\delta_{kn} L_{sn} D^2}{4\gamma} \frac{\sqrt{\sigma} \sin^2 x_n}{B\Lambda}, \quad (8)$$

where Λ is defined as

$$\Lambda = 1 - \sqrt{\sigma}\delta_{kn} + \frac{1}{2}\sigma\delta_{kn}^2. \quad (9)$$

The thermal conductivity term in Eq. (7) has been neglected. The performance of the stack is expressed in terms of the coefficient of performance

$$\mathrm{COP} = \frac{Q_{cn}}{W_n}. \quad (10)$$

5. Optimization of the stack

In the COP calculations, the data shown in Table 3 are used. Fig. 4 shows the performance calculations as a function of the normalized stack length L_{sn}, for different normalized stack positions x_n. The normalized position $x_n = 0$, corresponds to the driver position (pressure antinode). In all cases the COP shows a maximum. For each stack length there is an optimal stack position.

As the normalized length of the stack increases, the performance peak shifts to larger stack positions, while it decreases. This behavior is to be understood in the following way: A decrease of the center position of the stack means that the stack is placed close to the driver. This position is a pressure antinode and a velocity node. Eq. (8) shows that the viscous losses (second term on the right) are proportional to the square of the acoustic velocity. Thus decreasing the velocity will result in a decrease of the losses and hence a higher COP.

It is concluded that the maximum cooling power may be expected at a position roughly halfway between the pressure antinode and pressure node [3]. In Fig. 5 the COP peak, the cooling power, and the acoustic power, calculated at the peak position, are plotted as functions of the stack length. The cooling power and the acoustic power increase while the COP decreases as function of the stack length and thus as function of the normalized stack center position. As can be seen from Fig. 5, for a normalized stack length above 0.35, the COP is smaller than one.

Considering the above remarks and for practical reasons, we have chosen for a normalized stack center position of $x_n = 0.22$ in our setup. To achieve optimum performance this requires a stack length of $L_{sn} = 0.23$ (Fig. 4). Expressed in terms of the normal stack center position and length, we have $x_s = 8$ cm and $L_s = 8.5$ cm. This is equivalent to place the hot end of the stack at a distance of 3.75 cm from the driver. Under these conditions the dimensionless cooling power is $Q_{cn} = 3.7 \times 10^{-6}$. Since the required cooling power is 4 W, Eq. (7) leads to a cross-sectional area $A = 12\ \mathrm{cm}^2$ which is equivalent to a radius of $r = 1.9$ cm for a cylindrical resonator. To pump 4 W of heat, the stack uses 3 W of acoustic power (COP = 1.3).

6. Resonator

The resonator is designed in order that the length, weight, shape and the losses are optimal. The resonator has to be compact, light, and strong enough. The

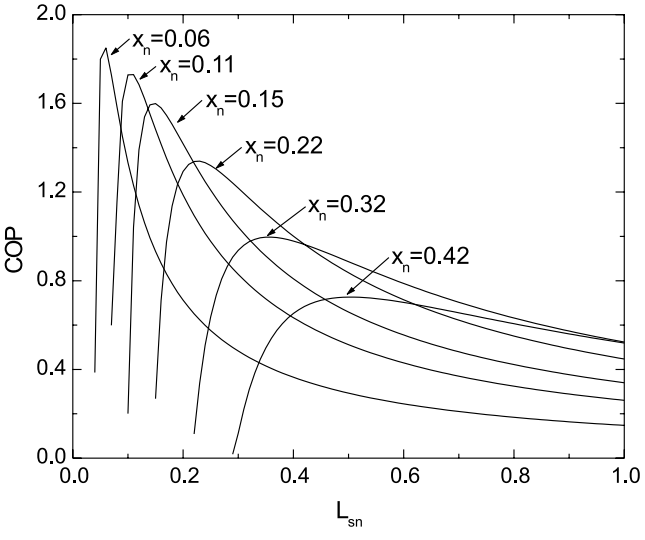

Fig. 4. Performance calculations for the stack, as a function of the normalized length and normalized center stack position.

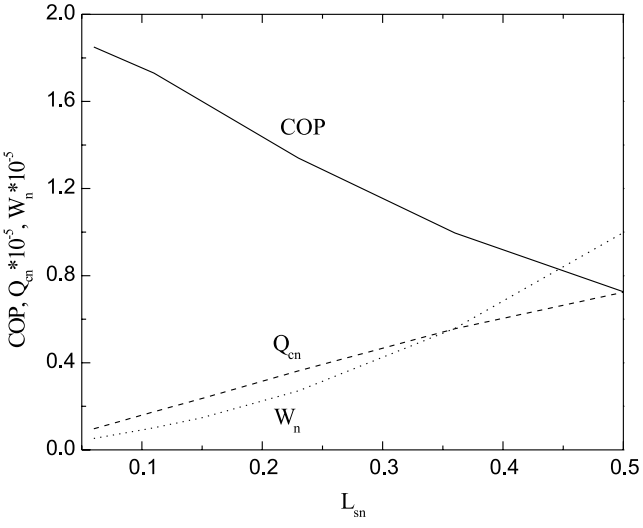

Fig. 5. The cooling power, acoustic power and performance at the stack center position of maximal performance, as a function of the normalized stack length.

shape and length are determined by the resonance frequency and minimal losses at the wall of the resonator. The cross-sectional area A of the resonator at the stack location is determined in the preceding section. The acoustic resonator can have a $\lambda/2$- or a $\lambda/4$-length, as shown in Figs. 6(a) and (b). The viscous and thermal relaxation dissipation losses take place in the penetration depths, along the surface of the resonator. In the boundary-layer approximation, the acoustic power lost per unit surface area of the resonator is given by [1]

$$\frac{d\dot{W}_2}{dS} = \frac{1}{4}\rho_m|\langle u_1\rangle|^2\delta_v\omega + \frac{1}{4}\frac{|p_1|^2}{\rho_m a^2}(\gamma-1)\delta_k\omega, \qquad (11)$$

where the first term on the right-hand side is the kinetic energy dissipated by viscous shear. The second term is the energy dissipated by thermal relaxation. Since the total dissipated energy is proportional to the wall surface area of the resonator, a $\lambda/4$-resonator will dissipate only half the energy dissipated by a $\lambda/2$-resonator. Hence a $\lambda/4$-resonator is preferable. Hofler [14] shows that the $\lambda/4$-resonator can be further optimized by reducing the diameter of the resonator part on the right of the stack (Fig. 6(c)). The way to do this is by minimizing Eq. (11). As shown in Fig. 6(c), two parts can be discerned, a large diameter tube (1) containing the stack with diameter D_1 and a small diameter tube (2) with diameter D_2. The losses in part (2) are plotted as function of the ratio D_1/D_2 in Fig. 7. The thermal loss increases monotonically as function of the ratio D_1/D_2, but the viscous losses decrease rapidly up to about

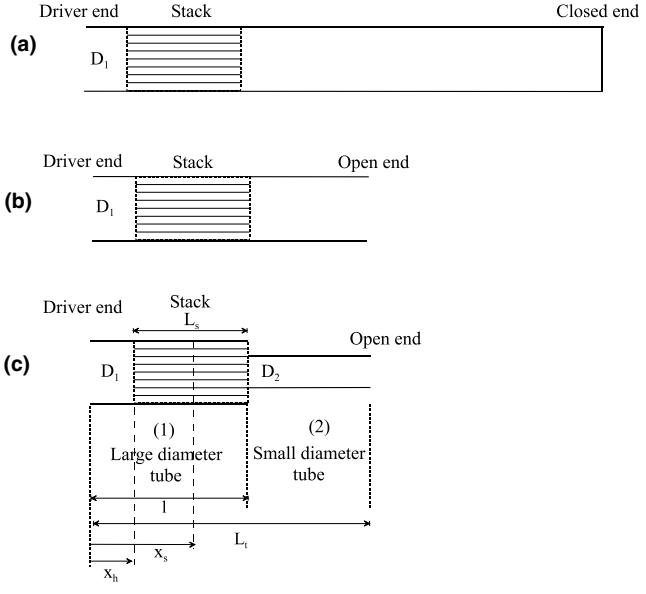

Fig. 6. Three type resonators showing the optimization of the resonator, by reducing the surface area: (a) a $\lambda/2$-tube; (b) a $\lambda/4$-tube; (c) an optimized $\lambda/4$-tube. The different dimensions used in the calculations are shown in (c).

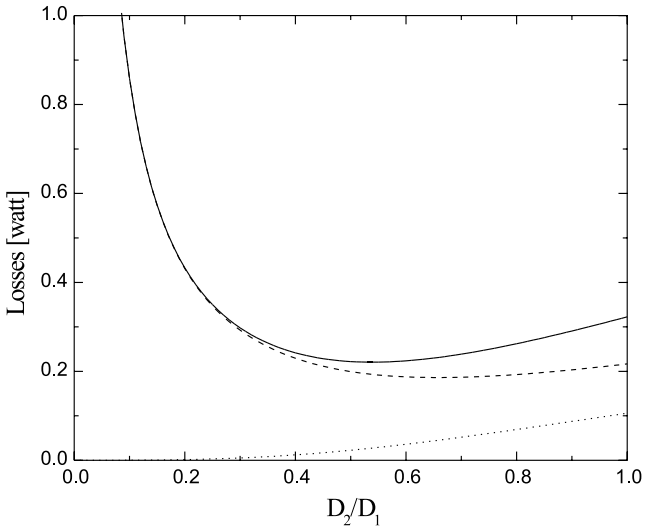

Fig. 7. The calculated losses in the small diameter resonator part (2), as functions of the ratio of the diameter of the small diameter tube to the diameter of stack resonator part (1). The dots are the thermal losses, the dashed-line is the viscous losses, and the solid plot represents the total loss. The total loss show a minimum at $D_2/D_1 = 0.54$.

$D_1/D_2 = 0.5$ and then increase slowly. As a result the total loss (sum) has a minimum at about $D_1/D_2 = 0.54$.

Hofler [14] and Garrett [15] used a metallic spherical bulb to terminate the resonator. The sphere had sufficient volume to simulate an open end. But at the open end, which is a velocity antinode, the velocity is maximum so that an abrupt transition from the small diameter tube to the bulb can generate turbulence and so losses occur. Taking into account this problem along with the requirement to keep the resonator compact we used a cone-shaped buffer volume to simulate the open end. The calculation optimization of the half-angle of the cone for minimal losses has been determined to be 9°. A gradual tapering is also used between the large diameter tube and small diameter tube. The final shape of our resonator is shown in Fig. 8. Measurements of the standing wave acoustic pressure distribution inside the resonator show that the system is nearly a quarter-wavelength resonator.

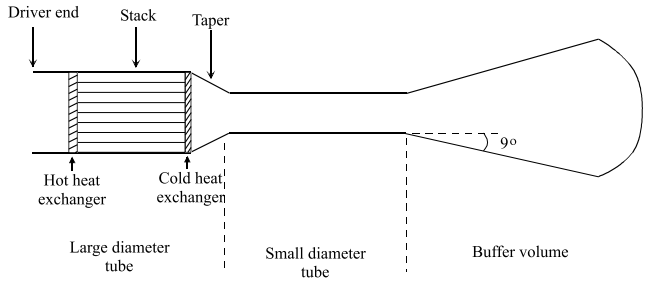

Fig. 8. The final shape used for the optimized resonator. It consists of a large diameter tube, containing a stack and two heat exchangers, a small diameter tube, and a buffer volume which simulates an open end.

So far we have determined the diameters of the large and small diameter tubes along with the length of the large diameter tube. The total length of the resonator is determined by the desired operation frequency of 400 Hz. By matching the pressure and volume velocity at the interface between the small diameter and large diameter tube one can deduce the resonance condition which can be used to control the length. By reference to Fig. 6(c), the amplitudes of the dynamic pressure and gas velocity due to the standing wave in the large diameter tube (1) are given by

$$p^{(1)} = p_0^{(1)} \cos(kx) \tag{12}$$

and

$$u^{(1)} = \frac{p_0^{(1)}}{\rho_m a} \sin(kx), \tag{13}$$

where the superscript (1) refers to the large diameter tube (1), and $p_0^{(1)}$ is the dynamic pressure amplitude at the driver location (antinode). Pressure and velocity in the small diameter tube (2) are given by

$$p^{(2)} = p_0^{(2)} \sin(k(L_t - x)) \tag{14}$$

and

$$u^{(2)} = \frac{p_0^{(2)}}{\rho_m a} \cos(k(L_t - x)), \tag{15}$$

where L_t is the total length of the resonator, and subscript (2) refers to the small diameter tube.

At the interface between the two parts at $x = l$, where l is the length of the large diameter tube (1), the pressure and the volume flow have to be continuous, this can be summarized by saying that the acoustic impedances have to match at the junction, thus

$$Z^{(1)}(l) = Z^{(2)}(l). \tag{16}$$

By substituting

$$Z^{(1)}(l) = \frac{p^{(1)}}{A_1 u^{(1)}} = \frac{\cot(kl)}{A_1} \tag{17}$$

and

$$Z^{(2)}(l) = \frac{p^{(2)}}{A_2 u^{(2)}} = \frac{\tan(k(L_t - l))}{A_2} \tag{18}$$

into Eq. (16), one obtains the resonance condition

$$\cot(kl) = \left(\frac{D_1}{D_2}\right)^2 \tan(k(L_t - l)), \tag{19}$$

where $L_t - l$ is the length of the small diameter tube. Substitution of D_1, D_2, l into Eq. (19) yields a total length of $L_t = 37.5$ cm, so that the length of the small diameter tube is 25 cm. In our calculations we did not take into account the presence of the stack, heat exchangers, tapering, and damping which influence the resonance frequency of the system and hence the length.

Straight tubes like that shown in Figs. 6(a) and (b) have resonance modes which are an integer number of the fundamental mode. Whenever nonlinear effects exist, higher harmonics may be generated which coincide with the resonance modes, and hence will be amplified. This means that energy transfer will take place from the fundamental operation mode to the higher oscillation modes. This loss mechanism is to be avoided in thermoacoustic devices. Eq. (19) shows that the resonance modes of the resonator having a non-uniform cross-section are not an integer number of the fundamental. In this way harmonics can be avoided. Hence, besides the benefit of reducing the losses, the optimized resonator shown in Fig. 8 has the advantage of having normal resonance modes which are not an integer number of the fundamental mode. Furthermore, Oberst [16] showed that, using resonators with a shape like that illustrated in Fig. 6(c), can lead to extremely strong standing waves with relatively pure wave forms.

As can be seen from Fig. 8, the large diameter resonator consists mainly of the stack and the two heat exchangers. Thus, the energy losses take place in these elements. The resonator losses are located at the small diameter tube. As can be seen from Fig. 7 the minimal power loss for $D_1/D_2 = 0.54$ is $\dot{W}_{res} = 0.22$ W. These losses are mainly caused by viscous losses. This energy loss shows up as heat at the cold heat exchanger (Fig. 1).

7. Heat exchangers

Heat exchangers are necessary to transfer the heat of the thermoacoustic cooling process. The design of the heat exchangers is a critical task in thermoacoustics. Little is known about heat transfer in oscillatory flow with zero mean velocity. The standard steady-flow design methodology for heat exchangers cannot be applied directly. Furthermore, an understanding of the complex flow patterns at the ends of the stack is also necessary for the design. Nowadays some research groups are using visualization techniques to study these flow patterns which are very complicated [17]. In the following, we will discuss some issues for the design of the heat exchangers.

7.1. Cold heat exchanger

The whole resonator part on the right of the stack in Fig. 8, cools down so a cold heat exchanger is necessary for a good thermal contact between the cold side of the stack and the small tube resonator. An electrical heater is placed at the cold heat exchanger to measure cooling power. The length of the heat exchanger is determined by the distance over which heat is transferred by gas. The optimum length corresponds to the peak-to-peak

displacement of the gas at the cold heat exchanger location. The displacement amplitude is given by

$$x_1 = \frac{u^{(1)}}{\omega} = \frac{p_0^{(1)}}{\omega \rho_m a} \sin(kx). \quad (20)$$

Substituting the data from Table 3, and $x = l = 12.5$ cm, gives $x_1 = 1.47$ mm. The optimum length of the cold heat exchanger is thus about $2x_1 = 3$ mm. To avoid as much as possible entrance problems of the gas when leaving the stack and entering the cold heat exchanger or vice versa (continuity of the volume velocity), the porosity of the cold heat exchanger must match the porosity of the stack. This implies that a blockage ratio of 0.75 has to be used in the design of the cold heat exchanger. Acoustic power is also dissipated in the cold heat exchanger. Eq. (8) can be used to estimate the dissipated power. Substituting the position of the cold heat exchanger $x_n = 0.33$, the length $L_{sn} = 0.008$ and $\Gamma = 0$ (uniform mean temperature), yields that the cold heat exchanger will dissipate $\dot{W}_{chx} = 0.2$ W.

7.2. Hot heat exchanger

The hot heat exchanger is necessary to remove the heat pumped by the stack and to reject it to the circulating cooling water. As discussed in the precedent section, the optimal length of the heat exchanger is equal to the peak-to-peak displacement amplitude of the gas at the heat exchanger location. But since the hot heat exchanger has to reject nearly twice the heat supplied by the cold heat exchanger, the length of the hot heat exchanger should be twice that of the cold heat exchanger (6 mm). Substituting the position of the hot heat exchanger $x_n = 0.10$, the length $L_{hn} = 0.016$ and $\Gamma = 0$ into Eq. (8), we obtain an estimation for the acoustic power dissipated in the hot heat exchanger which is $\dot{W}_{hhx} = 0.33$ W.

8. Acoustic driver

The driver has to provide the total acoustic power used by the stack to transfer heat and dissipated in the different parts, thus

$$\dot{W}_t = \dot{W}_s + \dot{W}_{res} + \dot{W}_{chx} + \dot{W}_{hhx} = 3.76 \text{ W}. \quad (21)$$

Taking into account the power dissipated in the different parts, the performance of the system becomes

$$\text{COP} = \frac{\dot{Q}_c}{\dot{W}_t} = 1.06. \quad (22)$$

This value is lower than the performance of the stack alone 1.33.

The optimization of the driver has been discussed elsewhere [3,18]. A higher performance of the driver leads to a higher performance of the whole refrigerator system. Furthermore, a high performance of the driver means that the necessary acoustic power can be obtained without using high electrical currents which can damage the coil.

9. DeltaE

A check of the assumptions of the short stack and boundary layer approximation shows that the stack length $L_s = 8.5$ cm is a factor four smaller than $\lambda/2\pi = 1/k = 0.37$ m, $\delta_k \approx y_0$, and $\Delta T_m = 70$ K is about a factor four smaller than the mean temperature $T_m = 250$ K. Regardless of the weakness of the second assumption, the results of the calculations done so far are good estimates for the optimization of the refrigerator. The computer program DeltaE [19] can be used to predict the performance of our refrigerator. DeltaE solves the exact thermoacoustic equations in a geometry given by the user, using the boundary conditions for the different variables. The refrigerator geometry shown in Fig. 8 is used and the results of calculations are given in Fig. 9.

The calculations have been done using a drive ratio $D = 2\%$, a constant hot temperature $T_h = 289$ K, a frequency $f = 409$ Hz, a stack length of 8.5 cm, and an average pressure $p_m = 10$ bar. Helium is used as working gas. Changing the distance between the stack and the driver changes the resonance frequency if the length of the small diameter tube is kept constant (Eq. (19)). Therefore, we have allowed the length of the small diameter to change so that the resonance frequency is kept constant at 409 Hz. The calculated cold temperature T_c and the performance relative to Carnot COPR as function of the heat load at the cold heat exchanger $\dot{Q}$, and for different positions x_h of the hot end of the stack from the driver end, are shown in Fig. 9. The COPR increases as the distance increases, reaches a maximum at a distance of about 4.2 cm and then decreases. The optimum cooling power, corresponding to the heat load at the position of maximum COPR, increases as function of the position. The explanation of the behavior of COPR and $\dot{Q}$ is the same as that given in Section 5. The cold temperature at the cold heat exchanger is nearly a linear function of the heat load. The slope of the line decreases as the distance from the pressure antinode (driver) increases, so that the lowest temperature at $\dot{Q} = 0$, increases as the distance increases. This is a consequence of the decrease of the critical temperature gradient, as discussed in [3]. The maximum COPR for $x_h = 4.2$ cm, shows an optimum around $\dot{Q} = 2.75$ W at a cold temperature $T_c = 229$ K. The calculations show that the dissipated acoustic power in the cold heat exchanger and in the small diameter resonator is 0.65 W so that the total cooling power at the cold end is about 3.5 W. Based on the above calculations we choose to use a

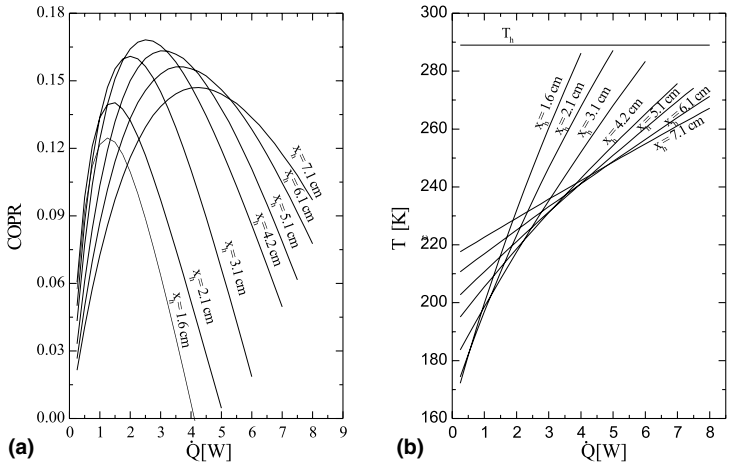

Fig. 9. DeltaE calculations as function of the heat load at the cold heat exchanger and for different positions from the driver: (a) performance relative to Carnot, COPR; (b) the cold heat exchanger temperature, T_C. The hot heat exchanger temperature T_h is also shown. The parameters used in the calculations are discussed in the text.

stack of length 8.5 cm placed at 4.2 cm from the driver. The construction of the thermoacoustic refrigerator will be described elsewhere.

10. Conclusion

The design procedure of a thermoacoustic refrigerator has been discussed. We began the design by using the approximate short-stack and boundary-layer expressions for acoustic power and heat flow. It was shown how the great number of parameters can be reduced using dimensionless parameters and making choices of some parameters. The optimization of the different parts of the thermoacoustic refrigerator has been discussed. The construction procedure of the cooler is described elsewhere [4].

References

[1] Swift GW. Thermoacoustic engines. J Acoust Soc Am 1988;84:1146–80.
[2] Wheatley JC, Hofler T, Swift GW, Migliori A. Understanding some simple phenomena in thermoacoustics with applications to acoustical heat engines. Am J Phys 1985;53:147–62.
[3] Tijani MEH. Loudspeaker-driven thermo-acoustic refrigeration. Ph.D. thesis, unpublished, Eindhoven University of Technology, 2001.
[4] Tijani MEH, Zeegers JCH, deWaele ATAM. Construction and performance of a thermoacoustic refrigerator. Cryogenics 2001 [submitted].
[5] Olson JR, Swift GW. Similitude in thermoacoustic. J Acoust Soc Am 1994;95:1405–12.
[6] Sergeev SI. Fluid oscillations in pipes at moderate Reynolds number. Fluid Dyn 1966;1:121–2.
[7] Merkli P, Thomann H. Transition to turbulence in oscillating pipe flow. J Fluid Mech 1975;68:567–76.
[8] Hino M, Kashiwayanagi M, Nakayama M, Hara T. Experiments on the turbulence statistics and the structure of a reciprocating oscillating flow. J Fluid Mech 1983;131:363–99.
[9] Akhavan T, Kamm RD, Shapiro AH. An investigation of transition to turbulence in bounded oscillatory Stokes flows. J Fluid Mech 1991;225:423–44.
[10] Tijani MEH, Zeegers JCH, de Waele ATAM. The Prandtl number and thermoacoustic refrigerators. J Acoust Soc Am 2001 [submitted].
[11] Swift GW. Thermoacoustic engines and refrigerators. Encyclopedia Appl Phys 1997;21:245–64.
[12] Pat Arnot W, Bass HE, Raspect R. General formulation of thermoacoustics for stacks having arbitrarily shaped pore cross sections. J Acoust Soc Am 1991;90:3228–37.
[13] Tijani MEH, Zeegers JCH, de Waele ATAM. The optimal stack spacing for thermoacoustic refrigeration. J Acoust Soc Am 2001 [submitted].
[14] Hofler TJ. Thermoacoustic refrigerator design and performance. Ph.D. dissertation, Physics Department, University of California at San Diego, 1986.
[15] Garrett SL, Adeff JA, Hofler TJ. Thermoacoustic refrigerator for space applications. J Thermophys Heat Transfer 1993;7:595–9.
[16] Oberst H. Eine Methode zur Erzeugung extrem starker stehender Schallwellen in Luft Akustische Zeits 1940;5:27–36;
English translation: Beranek LL. Method for Producing Extremely Strong Standing Sound Waves in Air. J Acoust Soc Am 1940;12:308–400.
[17] Wetzel M, Herman C. Experimental study of thermoacoustic effects on a single plate. Part I: Temperature fields. Heat Mass Transfer 2000;36:7;
Wetzel M, Herman C. Part II: Heat transfer. Heat Mass Transfer 1999;35:433–42.
[18] Tijani MEH, Zeegers JCH, de Waele ATAM. A gas-spring system for optimizing loudspeakers in thermoacoustic refrigerators. J Appl Phys 2001 [submitted].
[19] Ward WC, Swift GW. Design environment for low-amplitude thermoacoustic engines. J Acoust Soc Am 1994;95:3671–4.